

# Tree bark re-identification using a deep-learning feature descriptor

Martin Robert, Patrick Dallaire, Philippe Giguère  
 Department of Computer Science and Software Engineering  
 Université Laval, Quebec City, Canada  
 martin.robert.3@ulaval.ca, {philippe.giguere,patrick.dallaire}@ift.ulaval.ca

**Abstract**—The ability to visually re-identify objects is a fundamental capability in vision systems. Oftentimes, it relies on collections of visual signatures based on descriptors, such as SIFT or SURF. However, these traditional descriptors were designed for a certain domain of surface appearances and geometries (limited relief). Consequently, highly-textured surfaces such as tree bark pose a challenge to them. In turn, this makes it more difficult to use trees as identifiable landmarks for navigational purposes (robotics) or to track felled lumber along a supply chain (logistics). We thus propose to use data-driven descriptors trained on bark images for tree surface re-identification. To this effect, we collected a large dataset containing 2,400 bark images with strong illumination changes, annotated by surface and with the ability to pixel-align them. We used this dataset to sample from more than 2 million  $64 \times 64$  pixel patches to train our novel local descriptors **DeepBark** and **SqueezeBark**. Our **DeepBark** method has shown a clear advantage against the hand-crafted descriptors SIFT and SURF. For instance, we demonstrated that **DeepBark** can reach a mAP of 87.2% when retrieving 11 relevant bark images, i.e. corresponding to the same physical surface, to a bark query against 7,900 images. Our work thus suggests that re-identifying tree surfaces in a challenging illuminations context is possible. We also make public our dataset, which can be used to benchmark surface re-identification techniques.

**Keywords**—Computer vision; Deep Learning; Local feature descriptor; Tree Bark; Instance retrieval; Metric learning;

## I. INTRODUCTION

The tracking of objects is important in many domains. For instance, tracking within the supply chain is a key element of the Industry 4.0 philosophy [11]. In the forestry industry, it would consist in re-identifying trees cut in the forest, when they arrive at the wood yard [16], for supply-chain tracking purposes. In the context of mobile robotics, being able to uniquely identify trees would improve localization in forests [15], [21]. Robots could use trees as robust visual landmarks, in order to localize themselves. In order to perform tracking on trees, one must be able to re-identify them, potentially from bark images. In this paper, we explore this problem by developing a method to compare images of tree bark and determining if they come from the same surface or not.

The difficulty of re-identifying bark surfaces arises in part from the self-similar nature of their texture. Moreover, the bark texture induces large changes in appearance when lit from different angles. This is due to the presence of deep troughs in the bark of many tree species. Another difficulty is the absence of a dataset tailored to this problem. There

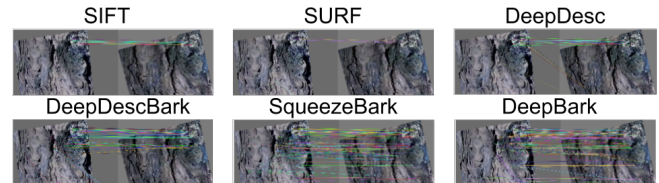


Figure 1. Qualitative matching performance of descriptors, for two images of the same bark surface. Every match shown in the image passed a geometric verification. Some false positive matches still remain, due to the high level of self-similarity. Notice the strong illumination changes between the image pair, a key difficulty in tree bark re-identification.

are already-existing bark datasets [10], [23], [6], but these are geared towards tree species classification.

To this effect, we first collected our own dataset with 200 uniquely-identified bark surface samples, for a total of 2,400 bark images. With these images, we produced a feature-matching dataset enabling the training of deep learning feature descriptors. We also have established the first state-of-the-art bark retrieval performance, showing promising results in challenging illumination conditions. In particular, it surpassed by far common local feature descriptors such as Scale Invariant Feature Transform (SIFT) [14] or Speeded Up Robust Features (SURF) [1], as well as the novel data-driven descriptor **DeepDesc** [19]: see Figure 1 for a qualitative assessment.

In short, our contributions can be summarized as follows:

- We introduce a novel dataset of tree bark pictures for image retrieval. These pictures also contain specific fiducial markers to infer camera plane transformation.
- Using our dataset and standard neural network architectures, we establish a new state-of-the-art performance for bark re-identification.

## II. RELATED WORK

Our problem is related to three main areas: *image retrieval*, *local feature descriptors* and *metric learning*, all discussed below. We also discuss the application of computer vision methods to the identification of bark images.

### A. Image retrieval

The problem of *image retrieval* can be defined as follows: given a query image, we seek other images in a database that look similar to the query one. In mobile robotics, an instance of this problem is known as Visual Place Recognition (VPR) [7], [8], where image retrieval is used to perform

localization. There, the objective is to determine if a location has already been visited, given its visual appearance. The robot could then localize itself by finding previously-seen and geo-referenced images. In the area of surveillance, the problem is defined as Person Re-Identification (Person Re-Id). It aims at following an individual through a number of security camera recordings [26]. This implies the ability to map multiple images of an individual to the same compact description, despite variation of view-point, illumination, pose or even clothes. Our tree bark re-identification is closest to this Person Re-Id problem, since we desire to track an individual bark surface despite changes in illumination and viewpoint.

### B. Local feature descriptor

To describe and compare images while being invariant to view point and illumination changes, we based ourselves on local feature descriptors. The goal of these descriptors is to summarize the visual content of a small image patch. The ideal descriptor is *a)* compact (low dimensionality) *b)* fast to compute *c)* distinctive and *d)* robust to illumination, translation and rotations. A popular approach is to use hand-crafted descriptors. They often rely on histograms of orientation and magnitude of image gradients, as in SIFT or SURF.

Recently, *data-driven* approaches based on machine learning have appeared [17]. Some learn a parametric function that maps image patches to compact descriptions that can be compared by their distance [5], [19]. Instead of describing an image patch alone, [24] takes two patches at once and directly provides a similarity probability. Some also propose a pipeline trained end-to-end (detector + descriptor) [9].

### C. Metric learning

To build a learned local feature descriptor, we turned to the field of metric learning. In this paradigm, one tries to learn a distance function between data points. More precisely, it seeks to make this distance small for similar examples, and large for dissimilar ones. This is in line with the points *c)* and *d)* of an ideal descriptor. This approach has been explored in [19], [9], where training relied on the so-called *contrastive loss*. Another line of work attempts instead to make the inter-class variation larger than the intra-class variation by a chosen margin in the vector space. This formulation corresponds to the *triplet loss* [18]. [22] instead chose to compare a similar pair of examples to multiple negative ones, using a clever batch construction process.

### D. Vision applied to bark/wood texture

Exploiting the information present in bark images has been explored before. For instance, hand-crafted features such as Local Binary Patterns (LBP) [12], [23], SIFT descriptors [10] and Gabor filters [27] have been used for tree species recognition. More closely related to our work, [3] compared variants of the LBP method for image retrieval,

but only at the species level. If bark is framed as a texture problem, one can find interesting work [25] that use ground textures such as asphalt or wood floor to enable robots to localize themselves. However, their technique is based on images with almost no variations. Moreover, each query is compared with one set of SIFT descriptions from their whole texture map. Data-driven approaches such as deep learning also were applied on images of bark, but strictly for species classification [6].

## III. PROBLEM DEFINITION

The problem we are addressing is an instance of re-identification. Given an existing database of bark images and a query image  $I_q$ , our goal is to find all images in the database that correspond to the *same physical surface*, in order to re-identify the tree, as seen in Figure 2. For instance, if the image compared to  $I_q$  is from the same tree *but* a different bark area, then it is not a valid match and the tree is not re-identified. We assume that  $I_q$  has a meaningful match in our database, i.e., we are not solving an open-set problem; See FAB-MAP [7] for novel locations detection.

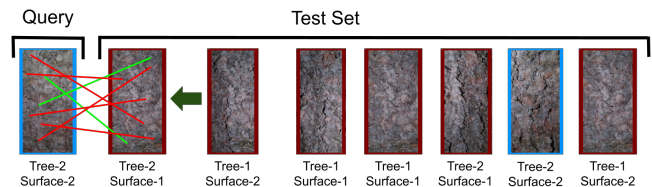


Figure 2. Here is a simplified example of bark images from two different trees, on which two different surfaces have been photographed. With two images per surface, this gives us eight images. Our goal is to take one bark image and retrieve the other bark image corresponding to the exact same surface. This way, we can recognize a previously-seen tree, using bark pictures as signature.

### A. Image global signature $s_i$

We perform the bark image search via global image signatures, defined as  $s_i = (K_i, V_i, b_i)$ . These signatures are extracted for each image (database and query  $I_q$ ), as depicted in Figure 3. For this, we mostly follow the method used in [20], summarized below. First, a keypoint detector extracts a collection  $K_i$  of keypoints from an image. For each of these keypoints  $k \in K_i$ , we extract a description  $v$  of dimension 128, yielding a list of descriptions  $V_i$ . These descriptions can be from standard descriptors, such as SIFT or SURF, or our novel descriptors, described further below. The remaining component of an image signature  $s_i$  is a Bag of Words (BoW) representation  $b_i \in \mathbb{R}^{1000}$ , calculated from the list of descriptions  $V_i$ . We also apply the standard *TF-IDF* technique. In [20], the comparison between two BoW is done using the cosine distance. Instead, we have  $l_2$ -normalized once every BoW as a pre-processing step and use the  $l_2^2$  distance to compare them. This way, our distance ranking is equivalent to the pure cosine distance, but without using a dot product.

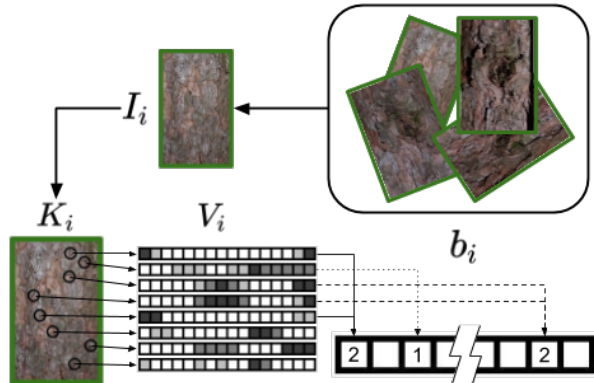


Figure 3. Illustration of the global signature  $s_i = (K_i, V_i, b_i)$  extraction pipeline, for a single image  $I_i$ . First, the keypoints  $K_i$  are detected. Then, for each keypoint  $k$ , a descriptor  $v$  is computed, creating the list  $V_i$ . Finally, a Bag of Words (BoW) representation  $b_i$  of  $V_i$  is computed from the quantization of all descriptions  $v$  via a visual vocabulary.

### B. Signature matching

The search is performed mainly by computing a score  $g$  between a query image signature  $s_q$  and each image signature  $s_i$  in the database, and retrieving the best match based on  $g$ . For the BoW technique, we simply use the distance between two BoWs  $\|b_q - b_i\|_2^2$  as our score  $g$ . Another way to calculate a score between  $s_q$  and  $s_i$  begins by taking the  $l_2^2$  distance between every description of  $V_q$  and  $V_i$  to obtain a collection  $M$  of putative matching pairs of features,  $m \in M = (v \in V_q, v \in V_i)$  with  $|M| = |V_q|$ . Then, we explored the use of two potential false match filters. The first one is the *Lowe Ratio (LR) test* introduced in [14]. The second one is a Geometric Verification (GV), which is a simple neighbors check. It begins by taking a match  $m = (v_x, v_y)$ , then retrieving the keypoints  $(k_x, k_y)$  associated with each description  $v$  of the match. Following this, we find the  $\alpha$  nearest neighbors of each of the keypoints in their respective images. Finally, the match is accepted if *at least*  $\rho\%$  of the  $\alpha$  neighbors of  $k_x$  have a match  $m \in M$  with the  $\alpha$  neighbors of  $k_y$ . The number of matches after filtering is then considered as the matching score  $g$ .

## IV. OUR APPROACH: DATA-DRIVEN DESCRIPTORS

Considering that tree bark highly-textured surfaces are problematic to hand-crafted descriptors, and the non-availability of datasets tailored to our task (see Table 1), we present here the main contribution of our paper, which is data-driven descriptors for bark image re-identification. First, we describe our novel bark image dataset. We then discuss how to process it in order to generate keypoint-aligned image patches required to train our descriptors. These descriptors are then described in detail, followed by training details.

### A. Bark Image Datasets

In order to develop our data-driven descriptors, we collected a dataset of tree bark images. To ensure drastic illumination changes, we took the pictures at night, and varied the position of a 550 lumen LED *Energizer<sup>TM</sup>* lamp. We

Reference	Number of images	Public	Instance Retrieval	Pixel Align
[27]	200			
[12]	300			
TRUNK12, [23]	393	✓		
[4]	540			
[2]	920			
AFF, [10]	1183			
BarkNet, [6]	23616	✓		
Ours	2400+750	✓	✓	✓

Table 1

Comparative of the existing bark datasets based on their size, availability, and applications. All datasets contain tree bark images designed for species classification, except ours. Adapted from [6].

also varied the position of the camera, an LG Q6 cellphone with a resolution of  $4160 \times 3120$  pixels. Since our training approach (subsection IV-B) requires keypoint-aligned image patches, we used fiducial markers on a wooden frame attached to trees to automate and increase the precision of the image registration, as shown in Figure 4.

We collected bark images for two different tree species, namely Red Pine (RP) (an evergreen) and Elm (EL) (a deciduous tree). For each species, 50 trees were selected, on which we further chose two different and distinct surfaces and took 12 photos for each of these surfaces. Each bark was surrounded by a custom-made wooden frame of  $50.5 \text{ cm}$  by  $15 \text{ cm}$ . We limited ourselves to only two species, to avoid positively biasing image retrieval results. Indeed, neural networks have the capacity to easily distinguish between tree species [6]. In total, we took 12 images per distinct surface with the aforementioned variations. To make our evaluation on EL bark more challenging, we also collected unseen bark images from elm trees without any markers. To keep these new images close to our original appearance distribution, we took them at night with three different illumination angles, but with limited changes in point of view. We collected a total of 30 images per tree for 25 trees with some physical overlap, spread nearly uniformly around the trunk. This gave us a total of 750 manually-cropped non-relevant images for any EL query taken at a scale similar to all of our other images.



Figure 4. Images from our database of the same surface of Elm (EL) bark, but for different illuminations and camera angles. In each image, there are four fiducial markers on a custom-made wooden frame, used for pixel-wise registration.

### B. Descriptor Training Dataset

Our descriptors require a dataset of  $64 \times 64$  patches for training with metric learning. Moreover, these patches not only need to be properly indexed per bark surface, they

must also be centered around the same physical location, corresponding to the keypoint. After automatically cropping the excess information from images (background, frame, shadow, etc), we performed registration between every image of a bark surface with a reference frame  $R$  via a homography  $H^r$ . We used the fiducial markers affixed to our wooden frame surrounding the bark surface (See Figure 4) to estimate these transformations. Then, for each bark image, we detected the maximum number of keypoints and projected them to the reference frame  $R$  via the homography  $H^r$ . We filtered all of the keypoints in  $R$  to require a minimum distance of 32 pixels between them to minimize overlap. This resulted in around 800-1000 distinct keypoints in  $R$ . For each of these keypoints, we then found the 12 image patches (one per image, see subsection IV-A) using a homography  $H^i$  that gives the transformation from the reference frame  $R$  to a specific bark image. This resulted in a collection of  $64 \times 64$  image patches corresponding to the exact same physical location on the bark, but with changes in illumination and point of view (rotation, scaling and perspective). Figure 5 shows three images of a unique bark surface, with the manual correspondence between keypoints. Figure 6 shows 12 examples of a keypoint extracted according to our algorithm used to create the training dataset.



Figure 5. Top row: pictures of the same bark surface with strong changes in illumination. Each circle color is a distinct keypoint. Bottom row: close up of the red keypoints from their respective images. This highlights the importance for a descriptor to be as immune as possible to such illumination changes.

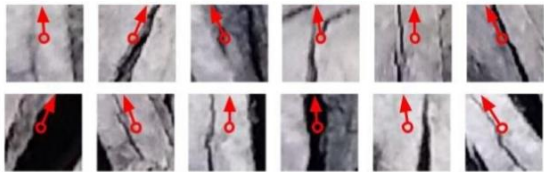


Figure 6. Actual example of  $64 \times 64$  patches of a keypoint. Red arrows indicate the orientation of the original bark images.

### C. DeepBark and SqueezeBark Descriptors

To perform description extraction, we implemented two different architectures with Pytorch 0.4.1. The first one, DeepBark, is based on a pre-trained version of ResNet-18 on ImageNet. We removed the average pool and the fully connected layers and replaced them with one fully connected layer (no activation function). The second one,

SqueezeBark, is a smaller network based on the pre-trained version of SqueezeNet 1.1 [13] on ImageNet. We again removed the average pool and the fully connected layers. We replaced them with a max pooling layer (to reduce the feature map) and a fully connected layer (no activation function). In both cases, the network computes a 128-dimensional vector, fed to an  $l_2$  normalization layer. Removing our last fully connected layer and calculating the number of parameters for the remaining convolutional layers, DeepBark is then composed of a total of 10,994,880 parameters and SqueezeBark includes 719,552 parameters. Our intention here is to be able to compare a number of network representation powers on the descriptor quality.

### D. Training details

To train our networks (DeepBark or SqueezeBark), we chose the N-pair-mc loss [22]. The only difference in our implementation is that, instead of using  $l_2$  regularization to avoid degeneracy, we  $l_2$ -normalized the descriptor vectors  $v$  to keep them in a hypersphere [18].

Our dataset is composed of  $64 \times 64$  patches around 70,800 distinct keypoints for the training set and 17,500 for the validation set for most of our experiments. Using 12 patches by keypoint for training and 2 for validation, this totals 884,600  $64 \times 64$  bark images patches. At each iteration, we only used a pair of examples for every keypoint in the training set. However, to ensure an equal probability for every patch to be seen together with every other patch, we randomly selected each patch tuple. We added online data augmentation in the form of color, luminosity and blurriness jitter. Each input image was normalized between  $(-1, 1)$  by subtracting 127.5 and then divided by 128. We optimized using Adam starting with a learning rate of  $1e^{-4}$  and reducing it by a factor of 0.5 each time the validation plateaued for 20 iterations.

We built the validation set by finding all keypoints in the bark images set aside for validation, and randomly selected 2 patches from the 12 available for each distinct keypoint. This gave us a fixed validation set, where every patch had a corresponding one. During training we validated our model by selecting 50 keypoints with their 2 examples at the time and performed a retrieval test to calculate the Precision at rank 1 (P@1). The final validation score was simply the average of every P@1 calculated for every batch of 50 keypoints. After training, we selected the model with the highest validation score. The training was stopped either with early stopping when the validation stagnated for 40 iterations, or when a maximum number of iterations was reached.

## V. RESULTS

Together with DeepBark and SqueezeBark, we evaluated hand-crafted descriptors, namely SIFT and SURF. We also included DeepDesc, a learned descriptor originally trained on the multi-view stereo dataset [5] and our re-implementation of DeepDesc renamed DeepDescBark,

which we train on bark data following our training procedure. All descriptors used the SIFT keypoint detector, except for SURF that used its own detector. For all experiments, we used a ratio of 0.8 for the LR test, and set  $\alpha = 15$  and  $\rho = 0.33$  for the GV filter. Also, each visual vocabulary *voc* was computed from the training images of each respective experiment, while being clustered using the *k*-mean algorithm.

Image retrieval can be evaluated in multiple ways. In our case, we favored metrics based on an ordered set, as they align best with our problem. Here are Precision at rank *K* (P@K) and Recall at rank *K* (R@K):

$$P@K = \frac{p(K)}{K}, \quad (1) \quad R@K = \frac{p(K)}{|I|}. \quad (2)$$

In Equation 1 and 2, *K* is a rank and the function *p* returns the number of relevant images ranked between the first rank and the *K* rank (*K* included). For Equation 2, *I* is the set of relevant images. We also present Precision Recall (PR) graph defined as:

$$PR = \{i \in I \mid (R@i_k, P@i_k)\}. \quad (3)$$

In Equation 3,  $i \in I$  represents one image and  $i_k$  is the rank where the image *i* can be found. Taking the mean of every  $P@i_k$  gives the Average Precision (AP). Keep in mind that these metrics are calculated for every query, averaged together. Thus, instead of AP we write mean Average Precision (mAP).

### A. Hyperparameters search

Our approach comprises three hyperparameters:  $\gamma$ ,  $\phi$  and  $\sigma$ . The first one,  $\gamma$ , is the maximum number of keypoints in an image. From experiments, increasing  $\gamma$  beyond 500 did not significantly improve the performance of any descriptor. The second hyperparameter is the downsizing factor  $\phi$  of the original image. Downsizing allowed the receptive field of any method to be increased, without changing its process. Our experiments showed that using  $\phi = 2$  generally helped every descriptor. Our third hyperparameter  $\sigma$  is the size of the gaussian kernel used in the blurring performed before passing the image through the keypoint detector. Note that the blur was used for the keypoint detection, but after that we used either the unblurred image to compute the description of learned descriptors (DeepBark, SqueezeBark, DeepDesc and DeepDescBark) or the blurred image for SIFT and SURF. The latter was necessary, as they used the keypoint information found on the blurred image. We found that the best blur filter value  $\sigma$  varied greatly between descriptors. The chosen values for the subsection V-C experiment are shown in Table 2. These values were found by averaging the results over 36 randomly-selected queries run on the validation set for each hyperparameter combination.

### B. Impact of training data size

Data-driven approaches based on Deep Learning tend to be data hungry. To check the impact of the training data

Descriptors	$\phi$	$\sigma$	mAP	Avg. Keypoint Num.
SIFT	1.5	3	0.406	469.4 $\pm$ 69.9
SURF	2.0	3	0.489	499.6 $\pm$ 4.8
DeepDesc	2.0	1	0.091	497.0 $\pm$ 17.4
DeepDescBark	2.0	0	0.076	492.8 $\pm$ 18.4
SqueezeBark	2.0	0	0.183	492.8 $\pm$ 18.4
DeepBark	2.0	0	0.966	492.8 $\pm$ 18.4

Table 2

Hyperparameters chosen after careful examination of the grid search, with the mean number of keypoints found at test time. The number of keypoints was capped to 500. mAP results shown have been obtained with the GV method. Some descriptors perform better with other scoring methods not shown here.

size, we created 5 training scenarios by tree species, which used 10%, 20%, 30%, 40% and 50% of the dataset. All trained descriptors were validated and tested on the same set (10% and 40% respectively) of each species dataset. We stopped training when the validation P@1 stagnated for 40 consecutive iterations.

Table 3 shows the performance of the descriptor DeepBark, for each training set size. For each species, the P@1, the R Precision (R-P) and the mAP are reported for the three scoring techniques: GV, LR and BoW. It is good to note that the BoW is also affected by the size of the training set, since the *voc* of the BoW is computed from that same training set. From these metrics, we concluded that performance gains were minimal beyond 40%. This confirmed that our training database is sufficiently large to obtain good performance. For references, when using 50% of RP as training data, we have access to approximately 42,700 distinct keypoints giving 512,000 bark image patches of  $64 \times 64$  pixels.

Red Pine						
	Metric	10%	20%	30%	40%	50%
BoW	P@1	0.971	0.985	0.985	<b>0.996</b>	0.994
	mAP	0.633	0.713	0.769	0.785	<b>0.812</b>
GV	P@1	0.988	0.990	<b>0.998</b>	0.996	<b>0.998</b>
	mAP	0.777	0.848	0.892	0.905	<b>0.922</b>
LR	P@1	<b>1.000</b>	<b>1.000</b>	<b>1.000</b>	<b>1.000</b>	<b>1.000</b>
	mAP	0.882	0.932	0.956	0.962	<b>0.967</b>
Elm						
	Metric	10%	20%	30%	40%	50%
BoW	P@1	0.940	0.956	0.971	0.979	<b>0.983</b>
	mAP	0.607	0.691	0.721	0.759	<b>0.764</b>
GV	P@1	0.944	0.965	0.977	0.981	<b>0.983</b>
	mAP	0.707	0.752	0.791	<b>0.816</b>	0.806
LR	P@1	0.985	0.996	0.998	0.998	<b>1.000</b>
	mAP	0.665	0.740	0.779	<b>0.800</b>	0.798

Table 3

Performance of the DeepBark descriptor, when training with 10%, 20%, 30%, 40% and 50% of the data from a single tree species. The remaining data has been used for validation (10%) and testing (40%). Hyperparameters were fixed through testing. Best results are in bold for each row.

### C. Descriptors comparison

We selected 50% of red pine bark surfaces and 50% of elm bark surfaces to create a test set, while using the remaining data for the training and validation sets. This corresponded to 80 unique bark surfaces for the training, 20 for the validation and 100 for testing, while keeping the ratio between tree species to 50/50 in each set. The data-driven descriptors

DeepBark, SqueezeBark and DeepDescBark were trained for 200 iterations, and we kept their model with the best validation. With 12 images for each bark surface, the test set had a total of 1200 images, with 600 per tree species. Each of these images was used as a query during the retrieval test. The results were averaged over all queries. We report results in Figure 7 as PR curves. This way, all 11 true positives are taken into account in our experimentation, properly estimating how well our approach resists to strong illumination/viewpoint changes.

From Figure 7, we can see that hand-crafted descriptors often successfully retrieve one image, but struggle beyond this. We can also see that DeepBark clearly dominates all descriptors. We can also notice that the precision is over 98% up to a recall of 6 images, when it is combined with GV. Interestingly, the results for SqueezeBark are mitigated. This might indicate that finding a good descriptor for bark images under strong illumination changes is a difficult problem, requiring a neural architecture with sufficient capacity. This is further supported by DeepDescBark exhibiting worse performance than SqueezeBark and DeepBark, which are larger networks. The very-low capacity of DeepDesc might also explain why it performed worse than SIFT or SURF at times. Finally, one can see that appropriate data improves performance, as demonstrated by the performance of DeepDescBark over DeepDesc.

#### D. Generalization across species

In the experiments of subsection V-C, we reported results on networks trained on both species, instead of training and testing each architecture on a single species. Our intention was to double the amount of training data and benefit from the potential synergy between species, which is often seen in deep networks (multi-task learning). Here, we precisely look at the generalization of our networks across species. We thus devised two experiments to evaluate the generalization from one species to the other and vice versa. The first one is composed of a training set with 80% of the RP data, using the remaining 20% as the validation set and all of the EL data as the test set (labelled RP->EL). We also performed the converse (EL->RP). We only report in Figure 8 the PR curve for the GV, as the trend is similar for other scoring methods. Figure 8 first shows that DeepBark is capable of generalizing across species, but that SqueezeBark do so to a lesser extent. Also, there is no clear trend for the generalization direction, since SqueezeBark generalized better from EL to RP but DeepBark generalized better in the opposite direction (from RP to EL).

#### E. Extra negative examples

To extrapolate how our system would perform on a larger database, we added 6,700 true negative elm examples with a crop size similar to query images. Half of them were original images, and the other images were generated via

data augmentation, by doing either a rotation, scale or affine transformation. Note that the original 3,350 images contain some physical overlap, as they come from 25 trees.

We reused the DeepBark network and the *voc* previously trained in subsection V-C. For the test, we removed the red pine images and kept the elm images that we separated into two crops (top and bottom halves) giving us a total of 1,200 images. We thus obtain a database of 7,900 bark images. Again, every query had 11 relevant images. This experiment is the only one where we split bark images into two crops, solely done to increase the database size. This has a negative impact on the performance, as the visible bark (and thus the number of visible features) is reduced by half. This can be seen by comparing Figure 7 and Figure 9.

	Metric	0	1600	6700
BoW	P@1	<b>0.952 ±0.214</b>	0.924 ±0.265	0.885 ±0.319
	mAP	<b>0.659 ±0.258</b>	0.572 ±0.276	0.491 ±0.281
GV	P@1	<b>0.998 ±0.041</b>	<b>0.998 ±0.041</b>	<b>0.998 ±0.041</b>
	mAP	<b>0.874 ±0.165</b>	<b>0.874 ±0.166</b>	0.872 ±0.168
LR	P@1	<b>0.999 ±0.029</b>	0.998 ±0.050	0.998 ±0.050
	mAP	<b>0.812 ±0.198</b>	0.794 ±0.209	0.768 ±0.223

Table 4

Results of the negative examples test for DeepBark. The number in the header indicates how many negative examples were added. The best results for each metric are in bold.

Among the three scoring methods evaluated, the most affected by the amount of negative examples was the BoW, as seen in Figure 9 and Table 4. The LR filter displays a smaller degree of degradation, as a function of the amount of extra negative examples. However, it still retains almost the same P@1. Finally, when looking at the GV, it is clear that the impact of extra negative examples is negligible. This again demonstrates the importance of performing GV filtering. We can thus conclude that our approach with GV would work on a much larger, realistic dataset.

#### F. Computing time considerations

Descriptors	R@25	R@50	R@100	R@200
SIFT-0	0.248	0.316	0.403	0.520
SIFT-6700	0.150	0.176	0.215	0.268
DeepBark-0	0.728	0.795	0.857	0.908
DeepBark-6700	0.561	0.625	0.681	0.739

Table 5

R@K for different values of K using the BoW. Results taken from the experiment with negative examples. The number beside the method names indicates how many negative examples were added.

Even if the LR test and the GV filter perform better, it is unrealistic to use them to search a whole database. Instead, the BoW can be used as pre-filtering to propose putative candidates to the other methods. To this end, we provide Table 5, which shows the R@K for various K for the BoW approach. These results suggest that keeping the 200 best matching scores calculated using the BoW on DeepBark would retain 73.9% of the 11 relevant images among 7,900

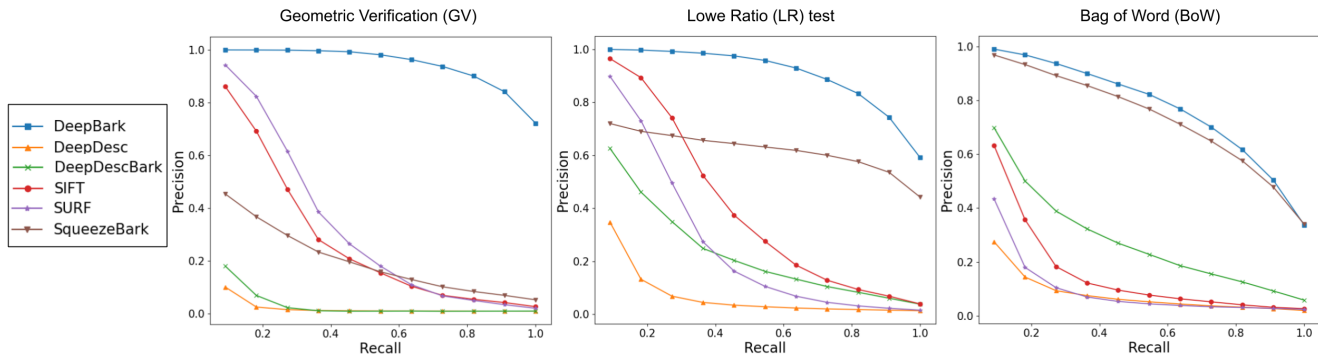


Figure 7. PR Curve for all descriptors tested on 50% of RP and EL. Learned descriptors were trained on the remaining 50% of bark. Each of the 1200 images of the test set is use as a query. No extra negative examples were added.

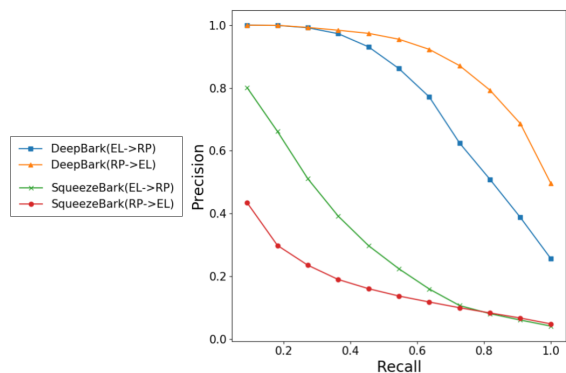


Figure 8. PR curve for the generalization test using the GV method. The arrow  $\rightarrow$  indicates the generalization direction (trained on  $\rightarrow$  tested on).

possible matches. As shown by [8], the BoW is fast to compare and can handle large datasets. To get a sense of the time that could be saved by the pre-filtering, we calculated the averaged time of 500 signature comparisons using our actual algorithms on a single thread of an Intel Core I-7. The BoW, GV, LR methods took respectively 0.002, 131.5 and 179.4 *ms* on averaged. It is important to note that the BoW technique could be sped up further using an inverted index and by taking advantage of its sparsity (on average 71.8% of it has a null entry in our experiments). From this, we can see that applying the GV on the  $K = 200$  top from the original 7,900 images can be accomplished in 35.88 *s*, while the BoW only took 0.016 *s* for the 7,900 images.

## VI. CONCLUSION

In this paper, we explored bark image re-identification in the challenging context of strong illumination and viewpoint variations. To this effect, we introduced a novel bark image dataset, from which we can extract over 2 million keypoint-registered image patches. Using the latter, we developed two local feature descriptors based on Deep Learning and metric learning, namely DeepBark and SqueezeBark. We showed that both our descriptors performed better than SIFT, SURF and DeepDesc on any of the three scoring methods presented. Our results indicate that using our descriptor DeepBark, retrieval is viable even for large datasets with

thousands of negative examples. Moreover, the approach can be sped up by using Bag-of-Words.

Our results are encouraging, but performance in a real-life scenario might differ. More data should be collected, in particular we should expand collection and testing on more tree species, as we have only tested generalization across one species to another. Also, it would be interesting to quantify the effect of the BoW size, the generalization capacity over more tree species or the effect of using other keypoint detectors. The training procedure could be further improved, in allowing for longer training, testing other networks, adding pre-training or using hard mining approaches.

## VII. ACKNOWLEDGEMENT

We would like to thank Marc-André Fallu for the access to his red pine plantation. The authors would also like to thank the "Fonds de recherche du Québec – Nature et technologies (FRQNT)" for their financial support. We are also grateful to Fan Zhou for his help in the data collection. Finally, we thank NVIDIA for their Hardware Grant Program.

## REFERENCES

- [1] Herbert Bay, Tinne Tuytelaars, and Luc Van Gool. SURF: Speeded Up Robust Features. In *CVIU*, volume 110, pages 404–417. 2006.
- [2] L. J. Blanco, C. M. Travieso, J. M. Quinteiro, P. V. Hernandez, M. K. Dutta, and A. Singh. A bark recognition algorithm for plant classification using a least square support vector machine. In *Int'l Conf. on Contemporary Comp.*, pages 1–5, Aug 2016.
- [3] Safia Boudra, Itheri Yahiaoui, and Ali Behloul. A comparison of multi-scale local binary pattern variants for bark image retrieval. In *ACIVS*, pages 764–775, 2015.
- [4] Adriano Bressane, Jose Arnaldo Roveda, and Antonio Martins. Statistical analysis of texture in trunk images for biometric identification of tree species. *Environmental monitoring and assessment*, 187:4400, 04 2015.
- [5] Matthew Brown, Gang Hua, and Simon Winder. Discriminative learning of local image descriptors. *T. PAMI*, 33(1):43–57, jan 2011.

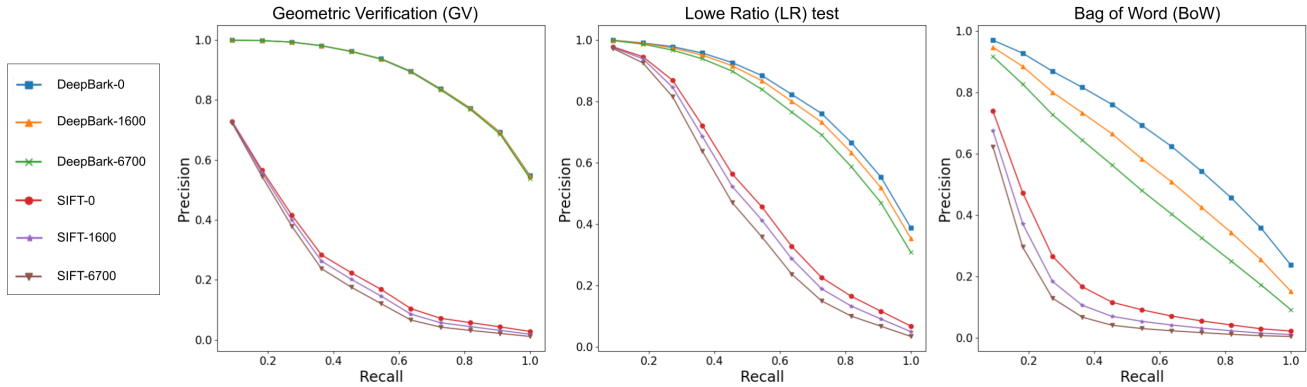


Figure 9. PR Curve for the negative examples test on SIFT and DeepBark. The number in the legend indicates how many negative examples were added.

- [6] Mathieu Carpentier, Philippe Giguère, and Jonathan Gaudreault. Tree species identification from bark images using convolutional neural networks. *IROS*, mar 2018.
- [7] Mark Cummins and Paul Newman. Fab-map: Probabilistic localization and mapping in the space of appearance. *IJRR*, 27(6):647–665, jun 2008.
- [8] Mark Cummins and Paul Newman. Highly scalable appearance-only slam - fab-map 2.0. In *RSS*, pages 1828–1833, jun 2009.
- [9] Daniel DeTone, Tomasz Malisiewicz, and Andrew Rabinovich. Superpoint: Self-supervised interest point detection and description. *CVPRW*, pages 337–349, 2018.
- [10] Stefan Fiel and Robert Sablatnig. Automated identification of tree species from images of the bark , leaves or needles. pages 67–74, feb 2010.
- [11] Ville Hinkka. Challenges for building rfid tracking systems across the whole supply chain. *Int'l Jour. of RF Tech. Res. and App.*, 3:201–218, 05 2012.
- [12] Zhi-Kai Huang, Zhong-Hua Quan, and Ji-Xiang Du. Bark classification based on contourlet filter features using rbpnn. In *Intelligent Computing*, pages 1121–1126, 2006.
- [13] Forrest Iandola, Song Han, Matthew W. Moskewicz, Khalid Ashraf, William Dally, and Kurt Keutzer. Squeezenet: Alexnet-level accuracy with 50x fewer parameters and <0.5mb model size. *CoRR*, abs/1602.07360, 02 2016.
- [14] David G. Lowe. Distinctive image features from scale-invariant keypoints. *International Journal of Computer Vision*, 60(2):91–110, nov 2004.
- [15] F. T. Ramos, J. Nieto, and H. F. Durrant-Whyte. Recognising and modelling landmarks to close loops in outdoor slam. In *ICRA*, pages 2036–2041, April 2007.
- [16] Sergey P. Sannikov and Vladimir V. Pobedinskiy. Automated system for natural resources management. *CEUR-WS*, May 2018.
- [17] Johannes L. Schonberger, Hans Hardmeier, Torsten Sattler, and Marc Pollefeys. Comparative evaluation of hand-crafted and learned local features. In *CVPR*, pages 6959–6968, jul 2017.
- [18] Florian Schroff, Dmitry Kalenichenko, and James Philbin. Facenet: A unified embedding for face recognition and clustering. In *CVPR*, pages 815–823, jun 2015.
- [19] Edgar Simo-Serra, Eduard Trulls, Luis Ferraz, Iasonas Kokkinos, Pascal Fua, and Francesc Moreno-Noguer. Discriminative learning of deep convolutional feature point descriptors. In *ICCV*, pages 118–126, dec 2015.
- [20] J. Sivic and A. Zisserman. Video google: a text retrieval approach to object matching in videos. In *ICCV*, number Iccv, pages 1470–1477 vol.2, 2003.
- [21] Nikolai Smolyanskiy, Alexey Kamenev, Jeffrey Smith, and Stanley T. Birchfield. Toward low-flying autonomous mav trail navigation using deep neural networks for environmental awareness. *IROS*, pages 4241–4247, 2017.
- [22] Kihyuk Sohn. Improved deep metric learning with multi-class n-pair loss objective. *NIPS*, (Nips):1857–1865,, 2016.
- [23] Matic Svab. *Computer-vision-based tree trunk recognition*. PhD thesis, Univerza v Ljubljani, 2014.
- [24] Xufeng Han, Thomas Leung, Yangqing Jia, Rahul Sukthankar, and Alexander C. Berg. Matchnet: Unifying feature and metric learning for patch-based matching. In *CVPR*, volume 07-12-June, pages 3279–3286, jun 2015.
- [25] Linguang Zhang, Adam Finkelstein, and Szymon Rusinkiewicz. High-precision localization using ground texture. *ICRA*, pages 6381–6387, 2017.
- [26] Zhedong Zheng, Liang Zheng, and Yi Yang. A Discriminatively Learned CNN Embedding for Person Reidentification. *ACM Trans. Multimedia Comput. Commun. Appl.*, 14(1):13:1–13:20, dec 2017.

- [27] Zheru Chi, Li Houqiang, and Wang Chao. Plant species recognition based on bark patterns using novel gabor filter banks. In *NIPS*, volume 2, pages 1035–1038, Dec 2003.